Journal of Sound and Vibration (1999) **221**(3), 415–441
Article No. jsvi.1998.1992, available online at http://www.idealibrary.com.on IDEAL

SOUND DIRECTIVITY GENERATED BY HELICOPTER ROTORS USING WAVE TRACING CONCEPTS

J. G. LEISHMAN

Department of Aerospace Engineering, Glenn L. Martin Institute of Technology, University of Maryland, College Park, MD 20742, *U.S.A.*

(*Received* 16 *February* 1998, *and in final form* 29 *September* 1998)

Results are presented from a study of directivity and sound focusing effects generated by helicopter rotors encountering parallel and oblique blade vortex interactions (BVI). The primary analysis is performed by using wave tracing to determine ray cones and acoustic lines from source points on the rotor with supersonic trace (phase) velocities. The results are compared and contrasted to predictions made from a numerical solution of the Ffowcs-Williams Hawkins equation. Sample problems considered include parallel and oblique BVI with an isolated line vortex, and interactions with self-generated epicycloidal vortices in forward flight. It is confirmed that the BVI process can produce strong directivity and clusters of focused sound waves in the far field. The trace velocity and wave tracing technique is shown to have potential applications for studies in noise reduction and/or noise directivity modifications using passive devices such as blade tip sweep. It is also shown that the numerically efficient nature of determining the primary acoustic lines with the trace velocity method can allow regions with strong directivity to be efficiently mapped out using redistributive observer point techniques.

1. INTRODUCTION

The noise intensity and directivity produced by helicopters is of considerable importance in both civilian and military operations, e.g., reference [1]. For example, there are certification and community noise constraints for take-offs and landings during civilian rotorcraft operations from vertiports. There is also a need to abate noise to reduce detectability in military operations. On helicopters the most obtrusive noise source is the main rotor, which can be heard both on the ground and in the cabin of the helicopter. A large proportion of this noise is generated by the unsteady aerodynamic interactions of the blades with tip vortices—the so-called blade vortex interaction (BVI) problem [2–4]. BVI noise can become particularly strong when the leading-edge of the blade becomes parallel to the axis of the tip vortex. This occurs primarily on the advancing and retreating sides of the rotor disk in forward flight. The BVI noise problem is

0022–460X/99/130415 + 27 $30.00/0

especially acute during descending low speed forward flight or during maneuvering flight, where the tip vortices can lie closer to the rotor plane.

A plethora of models exist to predict helicopter rotor acoustics, these ranging from analytic wave tracing methods to two-dimensional blade element type unsteady aerodynamics models coupled with Ffowcs-Williams Hawkins (FWH) methods, to modern computational fluid dynamics (CFD) coupled with Kirchhoff methods, e.g., references [5, 6]. However, it has not yet proven possible to model the aeroacoustics of a complete helicopter rotor to the fidelity necessary for acceptable predictions at reasonable computing costs, e.g., reference [7]. Much of the recent work on modelling the aeroacoustic effects of BVI has concentrated on CFD solutions. Complete first-principles based CFD approaches for aeroacoustics are not yet practical, in part, because of significant numerical dissipation and dispersion errors [8]. Furthermore, while coupled CFD and Kirchhoff based methods have provided significant insight into rotor aeroacoustic phenomena [9, 10], they are still only research tools and far too computationally expensive for routine use or parametric studies. Bearing in mind that any aeroacoustic model must be properly coupled to a structural dynamic model of the rotor blades, perhaps with some form of active control, there are clearly many limitations on what practical level of acoustic predictive capability can be genuinely achieved in the short term.

One complexity of the sound field produced a helicopter rotor cannot be underestimated. The highly three-dimensional unsteady aerodynamics produced by BVIs on the blades give rise to multiple noise sources with different directivity and phase relationships. The net sound field, therefore, comprises complicated interfering, and sometimes highly focused, acoustic wave paths. Besides the high computational cost of the rotor aerodynamics themselves, which may involve the use of numerically expensive free-vortex wakes [11, 12], the cost of the acoustics results from the repeated evaluation of the sound pressure at many observer locations. A typical SPL directivity calculation using a FWH or Kirchhoff acoustic method may use 10 000 or more observer points. Because the directivity is generally not known *a priori*, a regular Cartesian or polar grid must be used to ensure adequate resolution of the sound field, and so it becomes very expensive to systematically map out the directivity of the critical regions in the acoustic field. Furthermore, because of the typically pronounced directivity associated with BVI noise there is a very real possibility that localized regions that experience sound focusing effects can be missed, even by using very large numbers of observer points. This may result in misleading comparisons between different rotors and/or at different flight conditions.

It will be clear that in the quest to reduce helicopter rotor noise, not only does the rotor noise intensivity and directivity need to be accurately predicted, but strategies need to be devised to either reduce or defocus the rotor sound. One approach is to try to relate the far-field rotor noise levels to their source points on the rotor. This has been recognized by several authors, including Strawn [10], Lowson [13] and Sim *et al*. [14]. Therefore, at least in principle, it may be possible to modify the aerodynamics at specific source points on the rotor and change the propagated noise in a profitable way. To this end, the use of higher harmonic cyclic

pitch [15] and active trailing edge flaps [16, 17] have been suggested to modify the unsteady airloads and alter the intensity of propagated BVI noise. Passive designs such as blade tip sweep have also been proposed to dephase rotor noise sources [18]. Operational techniques such as aircraft trajectory optimization or tip-path-plane angle of attack control proposed by Schmitz [19], may offer such benefits in changing vortex/blade miss distances. However, any approach requires an understanding of the nature and focusing characteristics of the critical sound sources generated by the rotor. It is to this end that the present work is directed.

2. METHODOLOGY

It is well known that the aerodynamic intensity of a BVI depends on the strength of the tip vortex, the distance from the blade to the tip vortex, and the orientation of the vortex to the blade. Another important factor, which has been expounded by Lowson [13, 20], Ringler *et al*. [21], Sim [14, 22] and Widnall [23], is that the trace (or phase) velocity of the BVI source point determines the primary directivity of the sound field. This is particularly so in regard to the formation of regions of highly focused noise [13]. In these regions, it is found that the sound waves that have their origin from clusters of source points with supersonic trace Mach numbers on the rotor arrive simultaneously (or nearly so) at the same observer location, thereby generating an acoustic convergence.

The principles of wave focusing on a ground plane from supersonic aircraft has been formally established by Onyenonwu [24, 25] in regard to sonic boom theory. Similar basic principles can be applied to the rotor problem by recognizing that the trace (or phase) velocities of the BVI intersection point between the blade and the axis of the vortex filament inside the rotor disk can, under many conditions, be supersonic [20, 21]. The consequences of this is that the fronts of the spherical sound wavelets generated at the BVI source points on the blades will accumulate along an envelope, similar to a Mach cone generated by a supersonic aircraft. This is shown schematically in Figure 1 for a rectilinearly moving supersonic point source. It is apparent that the principal direction of the sound wave front propagation will be normal to the Mach one.

On a rotor, the trace Mach number, M_{tr}, is related to the relative speed of convection of the blade tip vortex axis relative to another blade, $U_T + U_V$, and the angle of intersection, γ, using

$$M_{tr} = \frac{U_T + U_V}{a \tan \gamma}, \tag{1}$$

where a is the sonic velocity. A diagram explaining the basic concept is given in Figure 2 for an axis system moving with the rotor. Note that for a rotor moving edgewise in forward flight the local velocity at the blade element is $U_T = \Omega R(r + \mu \sin \psi_b)$, where Ω is the angular rotational speed of the rotor, R is the rotor radius, r is the non-dimensional radial distance from the rotational axis, ψ_b is the blade azimuth position measured from the downstream pointing x-axis, and μ is the advance ratio (translational forward speed/ΩR). The term U_V in equation (1) is the additional local in-plane convection speed of the vortex

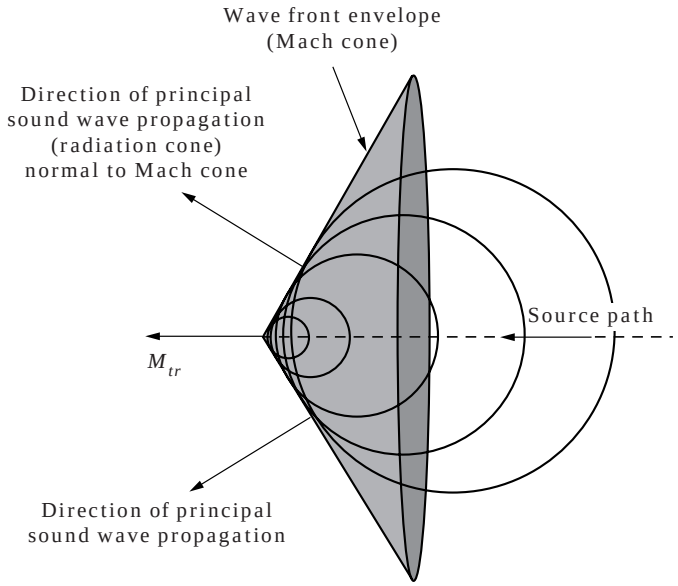

Figure 1. For a supersonic source the accumulated wave fronts will appear along an envelope that defines the principal direction of sound propagation.

filament, which arises from the self-induced effects of the vortical rotor wake or from the aircraft maneuver kinematics.

It will be apparent from equation (1) that the trace Mach number can range from subsonic to supersonic, and the trace velocity vector can be directed outward or inward along the blade axis. If the angle of intersection is small, i.e., the blade

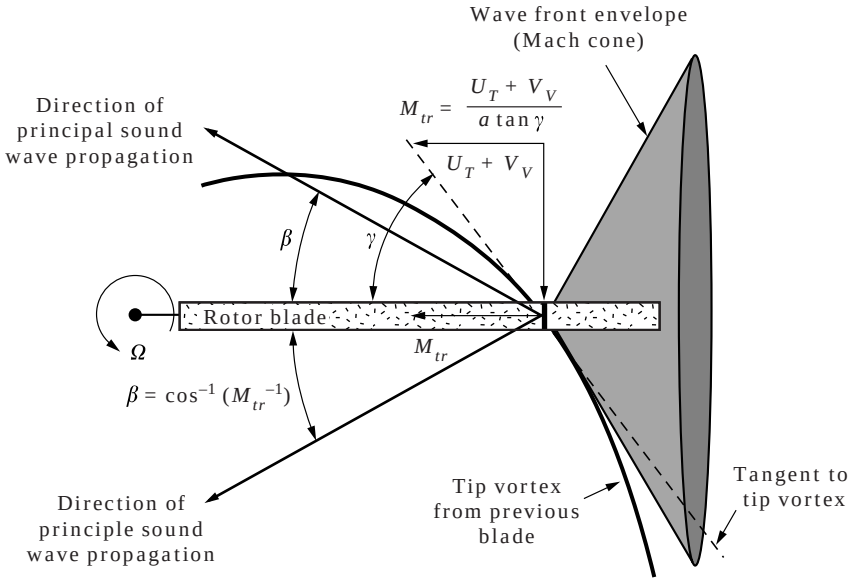

Figure 2. Schematic of trace (phase) Mach number concept for a radially inward moving supersonic BVI source point. Trace velocity is measured relative to co-ordinate system moving with the rotor.

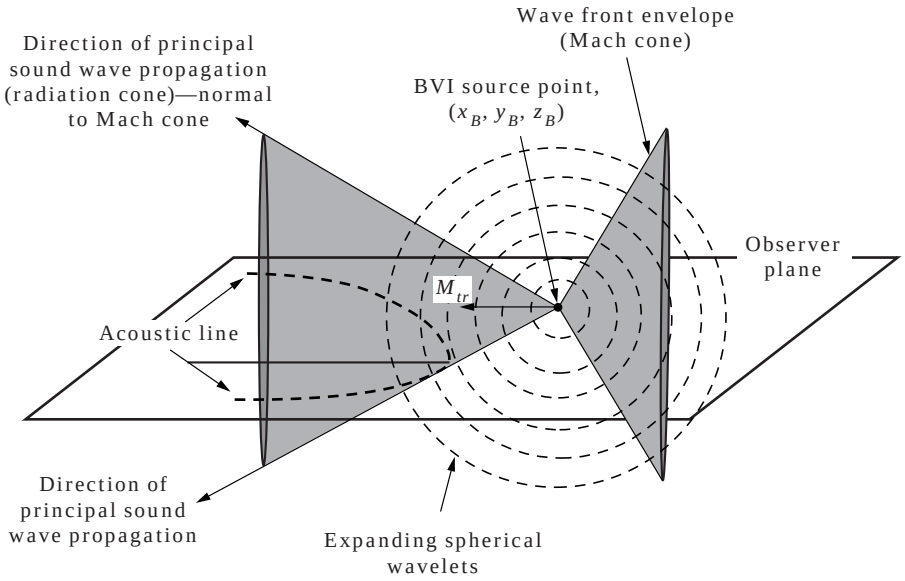

Figure 3. Schematic showing conic intersection (acoustic line) on observer plane of spherically expanding waves generated at a BVI point with supersonic trace velocity.

and vortex axes are almost parallel to each other, then the trace Mach number along the blade axis can be significantly supersonic. Figure 2 shows that the accumulated wavelet fronts propagate into the acoustic field along a ray cone with a semi-vertical angle β to the instantaneous trace velocity vector where

$$\beta = \cos^{-1}(M_{tr}^{-1}). \tag{2}$$

Because the value of β will vary from point to point on the blade, this effectively forms a series of intersecting ray cones with different vertices and spread angles.

It is usually desirable to examine the rotor acoustics on a horizontal (ground) plane below the rotor in a frame of reference where the observer moves with the rotor. When the ray cones generated from each supersonic BVI source point in the rotor plane intersect the horizontal ground plane they become conics; see Figure 3. For example, if the rotor plane is assumed to lie in the $z = 0$ plane parallel to the ground then for hovering flight the conic is a hyperbola with two open-ended segments of spread angle 2β. For a BVI source point at (x_B, y_B, z_B) the equation of the ray cone relative to the blade axis system can be written as

$$(x - x_B)^2 + (z - z_B)^2 = \frac{(y - y_B)^2}{c^2}, \tag{3}$$

where $c = (\tan\beta)^{-1}$. This cone intercepts a horizontal x–y observer plane at $z = k =$ constant, so the equation of the hyperbola in this plane is simply

$$(x - x_B)^2 + (k - z_B)^2 = (y - y_B)^2 \tan^2\beta. \tag{4}$$

The result is then transformed from the blade axis system to the rotor hub axis system. This planar intercept is termed an acoustic line because it forms the locus of any acoustic disturbances from the wave fronts that reach the x–y observer

plane from the BVI emission points. Note that in forward flight, the radiation cones become distorted by the local flow velocities, although the principal means of calculating the acoustic lines is the same. By formulating the orientations and intersections of these acoustic lines, which becomes mostly a problem in analytic geometry, it gives a measure of the qualitative directivity of the dominant sound in the far field as produced by the BVI events on the rotor. This is the essence of the so-called "radiation cone" methods originally formalized by Ringler *et al*. [21] and Sim *et al*. [14, 22]. It does not, however, permit a full directivity calculation nor a quantification of the acoustic intensity from the rotor. This is only possible using a FWH or Kirchhoff method with a strength assigned to each source point, i.e., the blade airloads.

Depending on the trace Mach number and direction of the trace velocity vector along the blade, it will be apparent the resulting acoustic lines in the x–y plane can lie at various orientations to each other and, in many cases, they may overlap. It is, therefore, possible for sound focusing to occur where the acoustic lines lie close together (high acoustic line density), and in some cases they may converge to form caustics. Ringler *et al*. [21] and Sim *et al*. [14, 22] state that caustics or intersections of ray cones result in wave focusing and the formulation of acoustic "hot spots". However, the intersection of acoustic lines (ray cones) is a necessary but not a sufficient condition to produce sound wave focusing. Intersections of acoustic lines as a means of determining locations of focused sound is only meaningful for wavelet fronts (rays) that have actually reached observer points at the same times, i.e., a retarded time calculation. Alternatively, to avoid a retarded time calculation the time of arrival of these sound wavelets at the x–y observer plane can be determined by using wave tracing from the BVI source (emission) point. This is the approach followed in the present work.

In a fixed reference frame with respect to the rotor the spherical wavelets that propagate radially from each BVI source point proceed at the local speed of sound plus the component of the flow velocity in the propagation direction, i.e., initially in the direction defined by β relative to the blade. For example, for an outward moving source point, the initial wavelet trajectory over a period Δt can be formalized as

$$x = x_B + (a\cos(\psi_b + \beta) + u)\,\Delta t, \qquad y = y_B + (a\sin(\psi_b + \beta) + v)\,\Delta t,$$
$$z = z_B + (a + w)\,\Delta t, \tag{5–7}$$

where ψ_b is the blade azimuth angle where the BVI event occurs and (u, v, w) can be considered the local velocities relative to the rotor (x, y, z) co-ordinate system. The initial conditions of the wavelets are defined by the emission times of all the individual sound fronts that are generated at BVI points with supersonic trace Mach numbers. By numerically computing the positions of the wavelets with respect to time, the pattern of fronts that intersect the x–y plane at any blade angle ψ_b can be determined. Note that after the wavelet intersects the observer plane, the principal direction of the front is along the acoustic lines. If the wave fronts approximately intersect in regions of high acoustic line density, then sound focusing can be said to occur.

3. RESULTS AND DISCUSSION

Wave tracing makes it possible to rapidly identify all the potential BVI locations over the rotor disk that contribute to the directivity of an important subset of the total rotor noise. Because mostly three-dimensional analytic geometry is involved, it can be done using relatively minimal computational resources. Alternatively, if the directivity of the rotor is known, such as from experimental measurements, the concept may also provide a means of tracking regions of high noise back to their BVI source points on the rotor disk. Aspects of this technique have been pursued to a limited extent by Lowson [13] and Strawn [10]. Such traceback ideas would seem to be a necessary precursor to understanding viable means of active acoustic control for the rotor. Yet, the complexity of the BVI problem, particularly for rotors with four or more blades, cannot be underestimated. Indeed, there are many local and groups of BVI events that occur over the rotor disk, and strong directivity (or other acoustic focusing) may arise from multiple regions on the rotor if the sound wavelets arrive at the observer location at the same time. Also, the intensity of these interactions will depend on several operational and geometric factors, including the rotor advance ratio, the number of blades, and the proximity of the rotor wake (the tip vortices) to the rotor. The latter will require a free-vortex wake model such as references [11, 12] for accurate calculations.

3.1. BVI'S WITH RECTILINEAR VORTICES

To reduce the uncertainties associated with the prediction of the strengths and locations of the blade tip vortices, simpler experiments have been conducted with non-lifting rotors and rectilinear vortices—see, for example, references [26–31]. These experiments have used rigid non-articulated one- or two-bladed rotors that encounter a controlled isolated streamwise vortex generated upstream of the rotor. The rotors were operated at nominally zero thrust, thereby minimizing the complexity of the problem resulting from the self-generated rotor wake and thereby allowing the effects of the generator vortex on the blade airloads and acoustics to be studied, essentially in isolation.

Kitaplioglu and Caradonna [30, 31] have measured unsteady blade loads with simultaneous microphone data. A two-bladed rotor with elastically stiff blades encountered a vortex with the vorticity vector parallel to the x-axis, and of known (measured) strength and location relative to the rotor. The hover tip Mach number was 0·7, and the rotor was operated at an advance ratio of 0·2. The primary BVI event occurred over the front of the rotor disk where the blade axis was effectively parallel to the axis of the generator vortex. While a BVI event may be expected downstream as well, the effects of the hub were shown by flow visualization to rapidly diffuse the vortex and effectively eliminated the BVI when $\psi_b = 0$.

Experimental data for the parallel interaction case ($y_v = 0{\cdot}0$) have been made available, and have been compared to predictions from various competing aeroacoustic models [6]. The agreement with test data has been found to be generally good for a number of vertical miss distances between the rotor and vortex. However, experimental measurements were not made at the regions in the acoustic field that exhibit strong directivity, nor were measurements made for oblique interactions with the generator vortex. This makes it difficult to fully assess

the complete quantitative predictive capabilities of all the various aeroacoustic models; because the large majority of BVIs on the rotor involve oblique interactions, it is important to understand their aeroacoustic effects. Aerodynamically, the oblique BVI cases produce significant three-dimensional unsteady airloads. Also, the directivity of the acoustics is somewhat more complicated because of the time-varying trace Mach numbers during the blade/vortex intersections.

The extension of the Kitaplioglu and Caradonna configuration to oblique BVIs provides a good challenge for any aeroacoustic method and, in the first instance, avoids the complexities of the real rotor wake. The obliqueness of the vortex to the blade can be obtained using various offset distances (y_v) between the vortex and the longitudinal axis. This means that the intersections of the vortex with the blades now occur at various orientations and blade azimuth angles. The radial location, r_v, of the BVIs can be found using

$$r_v = \left| \frac{y_v}{R \sin \psi_b} \right| \qquad \text{for } 0 \leqslant r_v \leqslant 1. \tag{8}$$

The corresponding trace Mach numbers are

$$M_{tr}(r_v, \psi_b) = \frac{M_{tip}(r_v + \mu \sin \psi_b)}{\tan \psi_b}, \tag{9}$$

where the blade/vortex intersection angle is $\gamma = \psi_b$ and $M_{tip} = \Omega R/a$. It is easily deduced that with increasing values of y_v fewer intersections points will have values of γ that result in supersonic trace velocities. For the special case where $y_v = 0$, the BVIs lie all along the blade at $\psi = (0, \pi)$ and $M_{tr} = \infty$ so that $\beta = \pi/2$.

The wave tracing technique allows for the rapid calculation of the principal sound directions and arrival times from all of the BVIs with supersonic source points. Typical results are shown in Figure 4 for the parallel interaction, and also with three lateral offset distances at $y_v = 0{\cdot}1$, $0{\cdot}3$ and $0{\cdot}5$. Results have been computed on a plane $3R$ below the rotor plane ($z/R = -3$), with the wavelet fronts generated by only one blade being shown to preserve clarity. The rotational axis of the rotor is at $(x, y) = (0, 0)$, and the free-stream velocity is from left to right. Note that although all these results represent a discretization of the problem into a finite number of radial blade elements and supersonic source points, each of the solutions in Figure 4 have been computed with the same resolution, and therefore, the concentration of acoustic lines and wavelet fronts can be compared directly. Also note, that while the sound wavelets produced by each supersonic source point are nominally circular in form, they have been plotted here discretely and so have a reduced angular resolution.

In the parallel case, which is shown in Figure 4(a), infinite trace Mach numbers occur all along the blade at $\psi_b = (0, \pi)$. The vortex of each ray cone is, therefore, located on the x-axis upstream and downstream of the rotational axis. The ray cones appear as hyperbolic acoustic lines on the horizontal observer plane, with

asymptotic slopes $\pm\tan^{-1}(1/M_{tip}\mu)$. Wave fronts of focused acoustic energy are formed by the intersection of the closely spaced spherical wavelets generated at each of the BVI source points with supersonic trace velocities. The position of these fronts at successive intervals in time (in this case every 2π rad of rotor revolution) can be tracked by the wave tracing algorithm described previously. Note that on the observer plane there are two sets of almost circular wavelets being generated, one from the BVIs occurring at the rear of the disk and the other occurring from the BVIs at the front. These BVI events occur half a rotor revolution apart. It will be seen that the primary wave fronts formed by the intersection of the individual groups of wavelets from each blade travel along the paths defined by the two sets of acoustic lines. Therefore, in the parallel BVI case, the sound wavelets become highly focused in directions perpendicular to the blades at $\psi_b = (0, \pi)$.

When the vortex is offset laterally from the longitudinal x-axis, the BVIs with the blades are no longer parallel. This means that there are fewer points along the blade that have supersonic trace Mach numbers. For example, for a starboard vortex offset, when the blade is in the first quadrant the locus of the BVI sweeps

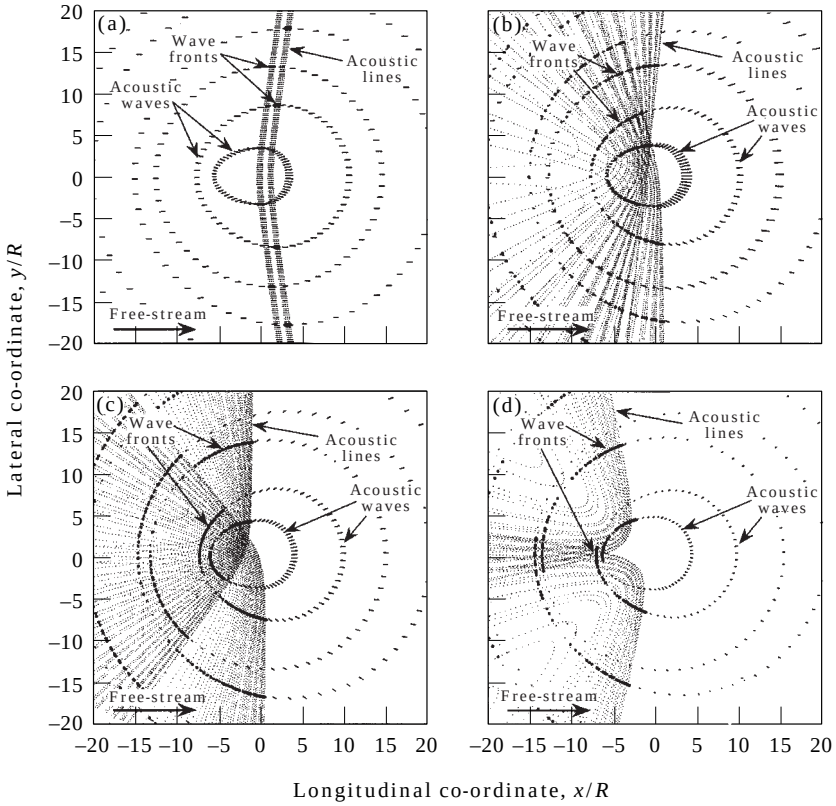

Figure 4. Acoustic lines and intersection wave fronts for a rotor interacting with an isolated streamwise vortex: (a) parallel interaction, $y_v = 0{\cdot}0$; (b) oblique interaction, $y_v = 0{\cdot}1$; (c) oblique interaction, $y_v = 0{\cdot}3$; (d) oblique interaction, $y_v = 0{\cdot}5$; $z = -3R$.

along the blade from the tip to the root; the intersection locus then moves from the root to the tip as the blade moves into the second quadrant. Because the trace Mach number also now varies along the length of the blade, the acoustic lines can no longer remain parallel to each other.

With reference to Figures 4(b)–(d), it can be seen that with a starboard vortex offset ($y_v > 0$) the acoustic lines are now directed toward the front of the rotor, i.e., into the second and third quadrants. In Figures 4(b)–(d) it will be seen that because of the varying supersonic trace Mach number in the oblique BVI cases, the focused sound waves radiate over a much larger spread angle. Again, the wave fronts formed by the intersection of wavelets from all the groups of source points with supersonic trace Mach numbers propagate along the acoustic lines when they reach the observer plane.

Figure 4(b) shows that only with a small offset of the vortex from the longitudinal axis ($y_v = 0{\cdot}1R$) the wave fronts are scattered in many directions, but have a primary focused region upstream of the rotor. Wherever there is a crowding of acoustic lines and wave fronts, increased sound pressures will occur. For this case, the sound is focused in the second and third quadrants, just upstream of the rotor hub (rotational axis).

Figure 4(c) shows that with a $0{\cdot}3R$ offset of the vortex, the spread angles of the radiation cones begin to decrease in accordance with the relationship $\beta = \cos^{-1}(1/M_{tr})$, so the acoustic lines and wave fronts become more crowded again. This results in acoustic energy that is radiated increasingly further forward of the rotor hub (rotational axis). Note that the wave fronts from each of the BVIs at the front and back of the rotor (which are separated in time by approximately half a rotor revolution) do not intersect. They do, however, appear to an observer as crowded wave fronts, albeit of alternating signs and intensities.

Figure 4(d) shows that with an offset of $y_v = 0{\cdot}5$ the BVIs are highly oblique. This means that there are relatively few points on the blades with supersonic trace Mach numbers; the trace Mach numbers are also correspondingly lower (equations (8) and (9)). Therefore, the spread angles of the acoustic lines are much smaller but the acoustic energy becomes somewhat more focused again. This observation emphasizes the fact that lower supersonic trace Mach numbers do not necessarily mean unfocused sound waves will occur.

The simple examples discussed above illustrate the highly directed nature of BVI noise, and the basic effects of obliqueness of the blade to the vortex axis on the sound radiation. The trace Mach number concept, however, does not allow for quantification of the effects of other BVI points that have subsonic trace Mach numbers or the wave intensities themselves, the latter requiring a relatively expensive calculation such as using a FWH method. Furthermore, in addition to BVI (dipole) effects, the thickness (monopole) sound pressures must be calculated to obtain the full acoustic field and confirm the sound directivity. This approach is considered next.

Results have been obtained using a numerical solution to the FWH equation [32] to obtain instantaneous acoustic field for the parallel ($y_v = 0{\cdot}0$) and oblique ($y_v = 0{\cdot}3$) blade vortex interactions [5, 33, 34]. In the present approach, which used

Farrasat's formulation-1 of the FWH equation [35], the fluctuating acoustic pressure, p', can be written as

$$p'(x, y, z, \psi) = \frac{1}{4\pi}\frac{\partial}{\partial t}\int\int\left[\frac{\rho v_n}{\mathscr{R}(1 - M_{\mathscr{R}})}\right]_{ret} \mathrm{d}S + \frac{1}{4\pi a}\frac{\partial}{\partial t}\int\int\left[\frac{l_{\mathscr{R}}}{\mathscr{R}(1 - M_{\mathscr{R}})}\right]_{ret} \mathrm{d}S$$

$$+ \frac{1}{4\pi}\int\int\left[\frac{l_{\mathscr{R}}}{\mathscr{R}^2(1 - M_{\mathscr{R}})}\right]_{ret} \mathrm{d}S, \tag{10}$$

where $\mathscr{R}$ is the distance from the source point to the observer, $l_{\mathscr{R}}$ is the total force on the fluid at each source point on the blade surface S in the direction of the observer, and *ret* indicates that the integrals are to be evaluated at the source or retarded time. The first term in equation (10) is the blade "thickness" noise and the second term is the "loading" noise. The third term is a near-field term, which does not represent a propagating wave. The quadrupole term has been neglected because for the BVI cases considered in this paper the Mach numbers are assumed subcritical.

The above form of the FWH equation is the same as that used in the Rotor Acoustic Prediction Program [36]. In the present work the equations are written in their convected form in a fixed frame with respect to the rotor. The present work is also different in that it uses a forward time calculation [33, 34]; that is, the time required to propagate the sound into the field (observer) point was calculated directly from the known emission times. While this gives results at unequally spaced observer times, the data can be readily sorted into discrete bins with the same reception time. A typical observer bin size is from one to one-half degrees of rotor azimuth (720 discrete acoustic bins per rotor revolution). If the observer time overlaps one bin width, then the acoustic information is weighted over adjacent bins by applying cubic weighting factors. After the complete noise signal is obtained at the observer location from all the sound sources, the time derivative on the appropriate terms in the FWH equation is taken using a central difference formula. The unsteady aerodynamics model for the airloadings was based on an indicial aerodynamic lift response and Duhamel superposition process [37]. The "thickness" noise was obtained using a standard source-sink displacement model [4, 36] to solve for the normal velocity, v_n.

The wave traces shown in Figures 5 and 6 vividly demonstrate the complex nature of the sound field even for this simplified BVI problem. Results were computed for a plane at $z/R = -3{\cdot}0$ and for 10 201 field points over a regular 101-by-101 polar grid out to $10R$ from the rotor axis. The "thickness" sound waves consist of crescent or spiral shaped wave fronts that spiral away from the rotor tips along characteristic curves. The BVI "loading" noise, for which a small separate contribution occurs for each BVI event along the blade, produces a series of closely spaced spherical wave fronts (see also Figure 4). These appear on the observer plane as a series of growing, almost circular, wavelets. Because the respective wave fronts have different intensities along their surface and also propagate at different orientations to each other, the combined effect is relatively complicated even for this simple geometrically well defined case.

In each case shown in Figures 5 and 6 the intensity of the two primary "loading" wave fronts are of opposite signs; one is of negative intensity and the other of positive intensity because the BVI airloads are reversed during the interaction on the front and back of the rotor disk. In the parallel case, the wave pattern is symmetrical but the sound waves are equal and opposite in strength. Therefore, in this case cancellation occurs along wavelet intersections, which is along the asymptotic acoustic lines $y = \tan(1/M_{tip}\mu)x$. This also corresponds to the region between the acoustic lines shown previously in Figure 4(a). Note that the spiral ("thickness" noise) and circular (BVI "loading" noise) wave fronts experience partial cancellation in some locations of the acoustic field but also reinforcement in other regions. This leads to a strong directivity pattern and is one reason why BVI noise cannot be studied completely in isolation; on an actual rotor both sources of noise will always be present.

For the oblique ($y_v = 0{\cdot}3$) case, the strongest BVIs occur at $\psi_b = 35$ and 145 degrees, and so produce waves that originate approximately 110 and 250 degrees apart in rotor azimuthal time. This produces a somewhat less symmetric wave pattern, but the essential wave pattern is the same as for the parallel case. Note, however, that the wave fronts are not of uniform intensity because a strength has been assigned to each BVI event on the blade; the time rates of change of lift have opposite signs at the front and back of the rotor. It will be seen in each case that the majority of the sound energy on the waves is clearly correlated within the regions previously defined by the acoustic lines (cf. Figure 4(c)).

The directivity can be further quantified by determining the time-averaged sound pressure level ($\mathrm{SPL} = 20 \log (p'_{rms}/p_{ref})$, where p'_{rms} is the rms pressure and $p_{ref} = 2 \times 10^5$ Pa) from the time-history of acoustic pressure at each observer point. These results are shown for the parallel case in Figure 7 and for the $y_v = 0{\cdot}3$ oblique case in Figure 8. Again, the data are for an x–y plane $3R$ below the rotor, with results being plotted from the rotor hub axis out to $10R$. These results show that the "loading" SPL in the observer direction is more upstream of the rotor. In both cases, however, the peak SPLs occur in directions perpendicular to the blade when it intersects the vortex axis. Clearly the FWH results verify the predictions of sound directivity made by the wave tracing method, although at a computational cost that is at least two orders of magnitude greater.

The SPLs resulting from "thickness" sources alone are the same for both the parallel and oblique cases—see Figures 7(b) and 8(b). This component of the sound is predominantly in-plane, and is distributed symmetrically above and below the rotor. For the current observer plane at $z/R = -3R$, the thickness noise only becomes significant for points well upstream of the rotor. The sound pressure resulting from the BVI loading is distributed asymmetrically above and below the rotor. The sign of the sound pressure changes depending on whether the observer is below or above the rotor plane; it also changes sign for the BVIs at the front and rear of the rotor. It will be noted that the SPL directivity from the combined "thickness" and "loading" contributions is such that they reinforce on the advancing side of the rotor and partially cancel on the retreating side—see Figures 7(c) and 8(c). This confirms an important limitation of the trace Mach number model. While numerically efficient in mapping the primary directivities of BVI

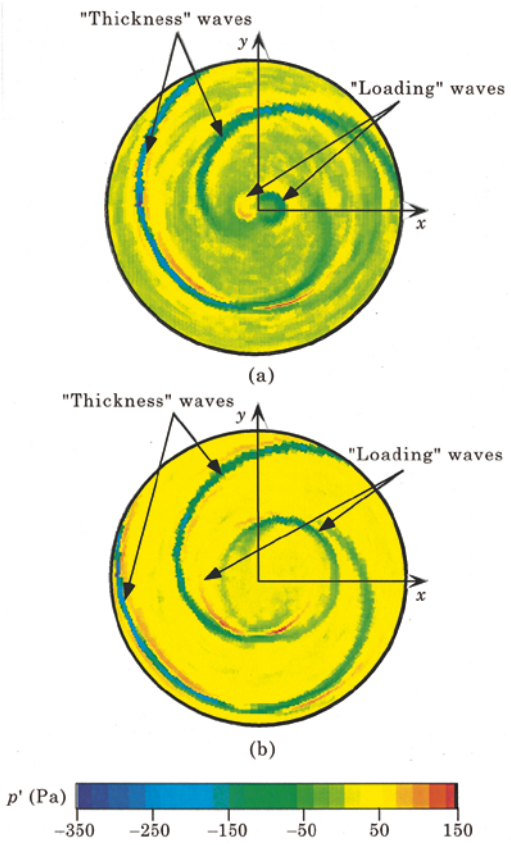

Figure 5. Propagation of acoustic waves for parallel BVI computed using FWH solution, $y_v = 0{\cdot}0$: (a) blade position, $\psi_b = 65$ degrees; (b) blade position, $\psi_b = 140$ degrees. Observer plane located $3R$ below rotor.

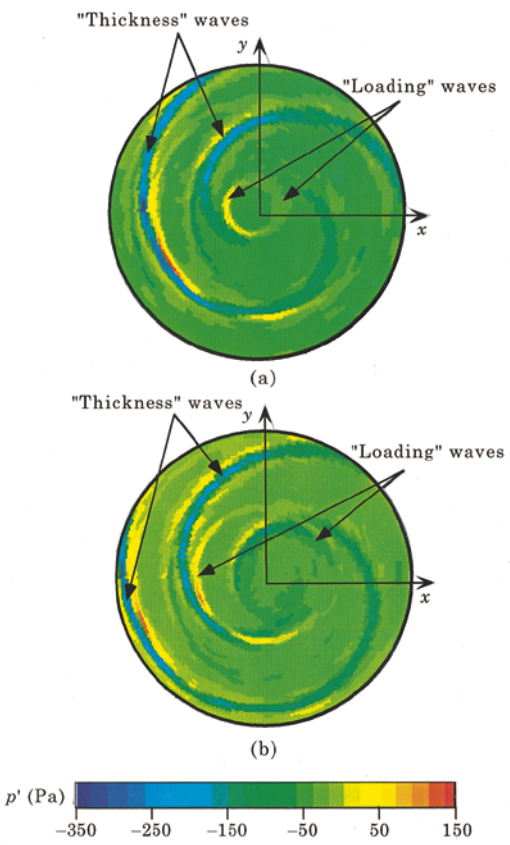

Figure 6. Propagation of acoustic waves for oblique BVI computed using FWH solution, $y_v = 0{\cdot}3$: (a) blade position, $\psi_b = 65$ degrees; (b) blade position, $\psi_b = 140$ degrees. Observer plane located $3R$ below rotor.

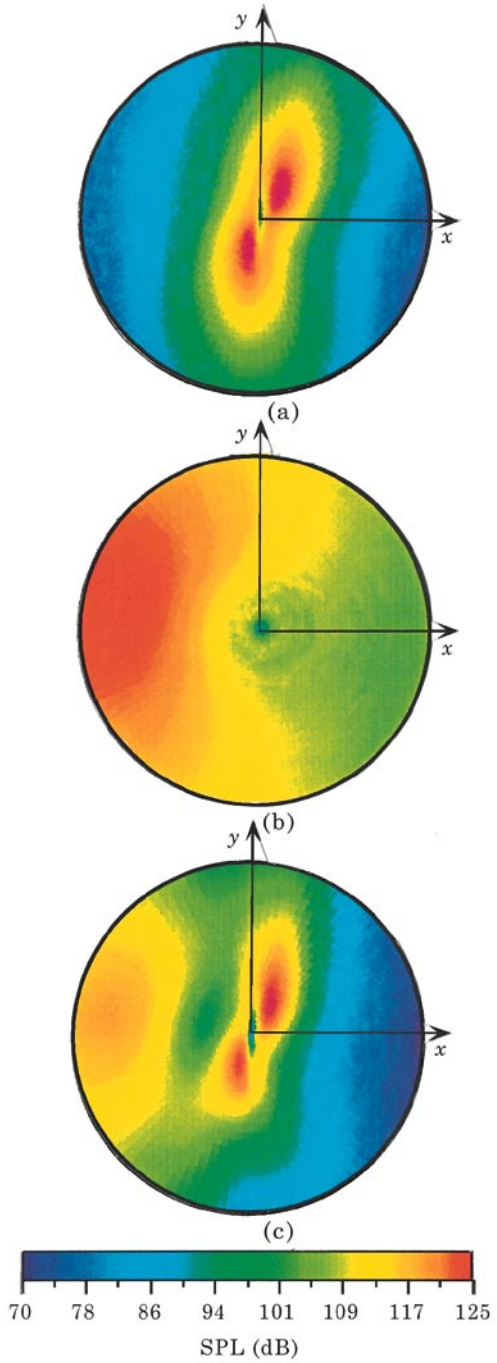

Figure 7. Distribution of SPL for parallel BVI, $y_v = 0{\cdot}0$, horizontal observer plane at $z/R = -3R$. (a) Loading noise, (b) thickness noise, (c) total noise.

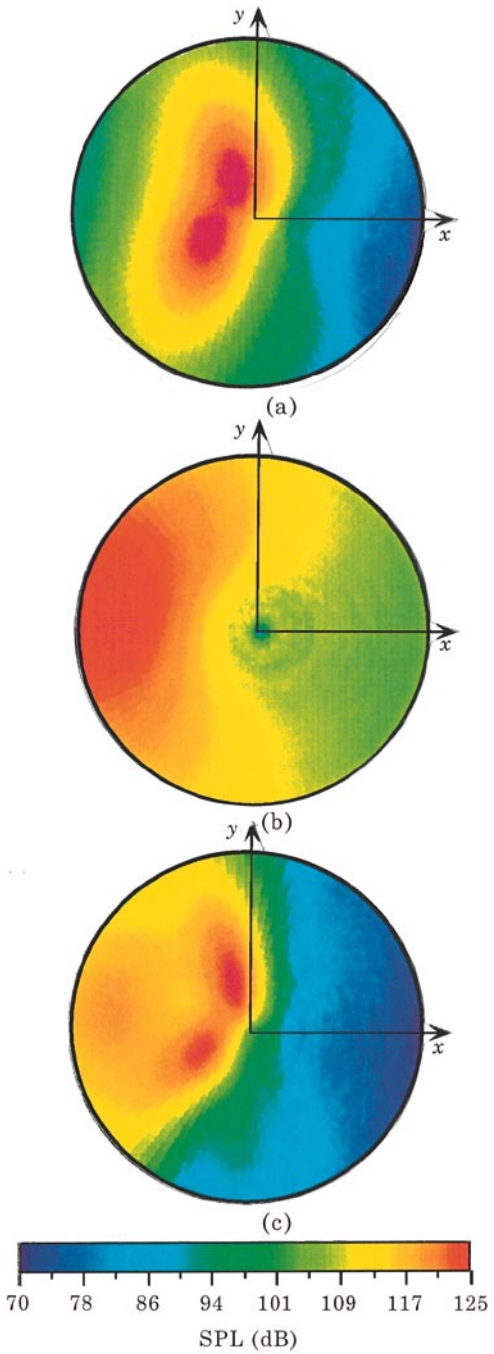

Figure 8. Distribution of SPL for oblique BVI, $y_v = 0{\cdot}3$, horizontal observer plane at $z/R = -3R$. (a) Loading noise, (b) thickness noise, (c) total noise.

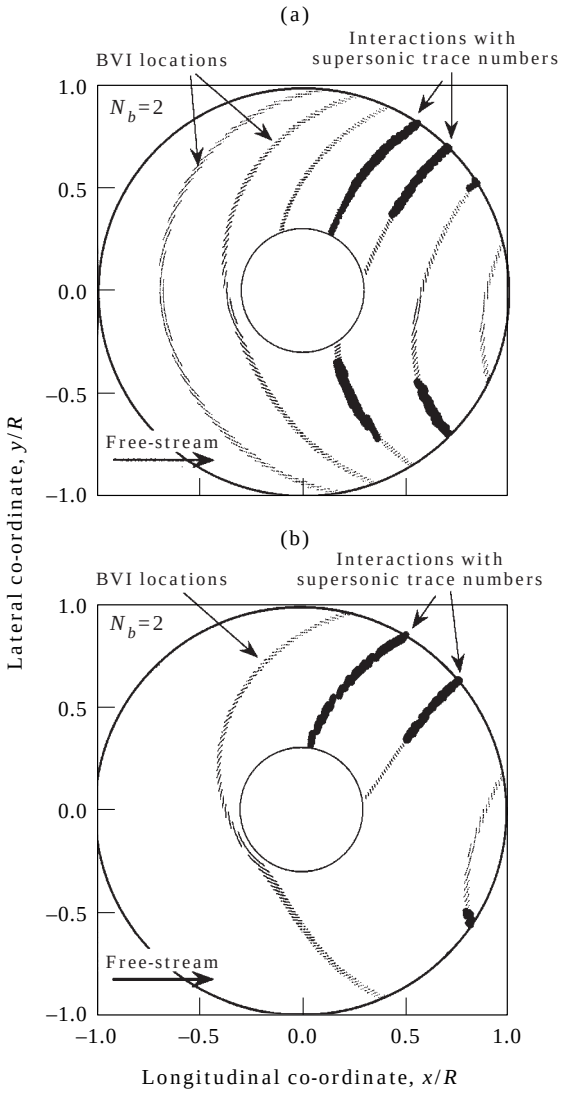

Figure 9. Locus of all possible BVI locations and the specific locations with supersonic trace Mach numbers for a two-bladed rotor operating in forward flight at advance ratios of (a) 0·1 and (b) 0·2.

noise, the effects of other noise sources such as blade "thickness" can significantly alter the net sound directivity from the rotor.

3.2. SELF-INDUCED BVI

The preceding cases are instructive but represent simplified conditions of focusing events found during parallel and oblique BVIs. In the real rotor case, the tip vortices trailed by the blades map out distorted epicycloidal paths and can intersect the blades at various orientations and vertical miss distances. For these self-induced BVIs, both the vortex/blade miss distance and the vortex/blade orientation affect the intensity (unsteady aerodynamics) of these interactions. Yet, as it has been shown, it is the orientation of the tip vortices to the blades that

affects the trace Mach number and, therefore, defines the primary direction of sound propagation.

When viewed from above, the trajectories of the tip vortex system trailed from a rotor in forward flight have a closely epicycloidal form. Generally, the tip vortex positions must be calculated by means of a free vortex wake model, for example, references [11, 12]. However, at higher advance ratios ($\mu > 0{\cdot}1$) the self-induced velocities in the plane of the rotor are small, so the tip vortex positions (x_w, y_w) relative in the x–y plane can be described by the parametric equations

$$x_w = R\cos(\psi_b - \zeta) + \mu R\zeta, \qquad y_w = R\sin(\psi_b - \zeta),$$

where ψ_b is the position of the blade and ζ is the age of the vortex element relative to the blade from which it was generated. For a rotor with N_b blades, each blade can potentially intersect the vortex trailed from any of the other blades. For an

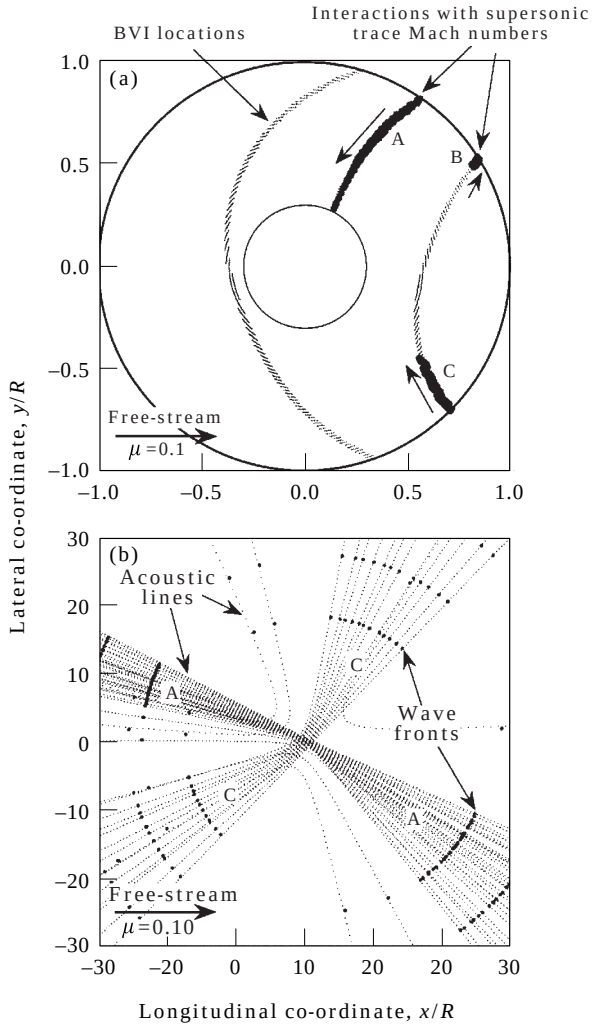

Figure 10. (a) BVI locations for a one-bladed rotor operating at an advance ratio of 0·1. (b) Corresponding acoustic lines and principal sound wave fronts.

undistorted wake structure (no self-induced effects), the intersection locations in the x–y plane can be determined purely from geometric considerations. For the ith blade, an intersection occurs if the equations

$$r \cos\left(\psi_b - \frac{2\pi(i-1)}{N_b}\right) = \cos(\psi_b - \zeta) + \mu\zeta,$$

$$r \sin\left(\psi_b - \frac{2\pi(i-1)}{N_b}\right) = \sin(\psi_b - \zeta).$$

are simultaneously satisfied, where ψ_b is the azimuth of the reference blade.

Lowson [13] describes how a solution to the preceding equations can be obtained analytically for an undistorted wake to determine the locus of all possible BVI locations. For the general case, where wake distortions from the epicycloidal form occur, especially when the helicopter undergoes maneuvering flight, the solution for the BVI intersection points must be determined numerically. This can be performed by discretizing the blade and the wake into small straight line elements, and then finding discrete BVI intersection points and also the direction of the trace velocity vector along the blade through simple analytic geometry. This is the approach followed for the calculations in Figure 9, which shows the locus of BVI locations and the specific locations with supersonic trace Mach numbers for a two-bladed rotor operating in forward flight at advance ratios (ratio of forward flight speed to rotor hover tip speed) of 0·1 and 0·2. Note that both the number of potential BVI locations and the number of points with supersonic trace Mach numbers significantly increases at low advance ratios.

For four or more rotor blades, the large number of potential BVI locations over the disk that have supersonic trace Mach numbers means the sound radiation pattern becomes relatively complicated. Therefore, representative results will now be shown for a one-bladed rotor. This more clearly illustrates how the sound waves and their principal directivities can, at least in principle, be related back to their azimuthal and radial source points on the blade. The use of a larger number of blades does not change the essential arguments to be made.

Results for an advance ratio of 0·1 are shown in Figure 10. In this case there are basically two significant BVI source clusters on the disk that have supersonic trave Mach numbers, one on the advancing side (cluster A) and one in the fourth quadrant (cluster C). Cluster B is insignificant acoustically. For both groups of BVIs the trace velocities are directed radially inward along the blade. Source cluster A has the highest sustained trace Mach number. This manifests as closely spaced acoustic lines all with a large spread angle ($2\beta \rightarrow \pi$) with wave fronts that propagate forward and to the right of the rotor. Cluster C interactions also have high trace Mach numbers, but with a time-varying gradient along the blade. This results in a somewhat more diffused sound radiation pattern from the third and first quadrants of the rotor disk.

Results for other advance ratios are shown in Figures 11 and 12. Figure 11 shows the BVI locations and regions on the disk with supersonic trace Mach numbers for a rotor operating at several advance ratios. Figure 12 shows the

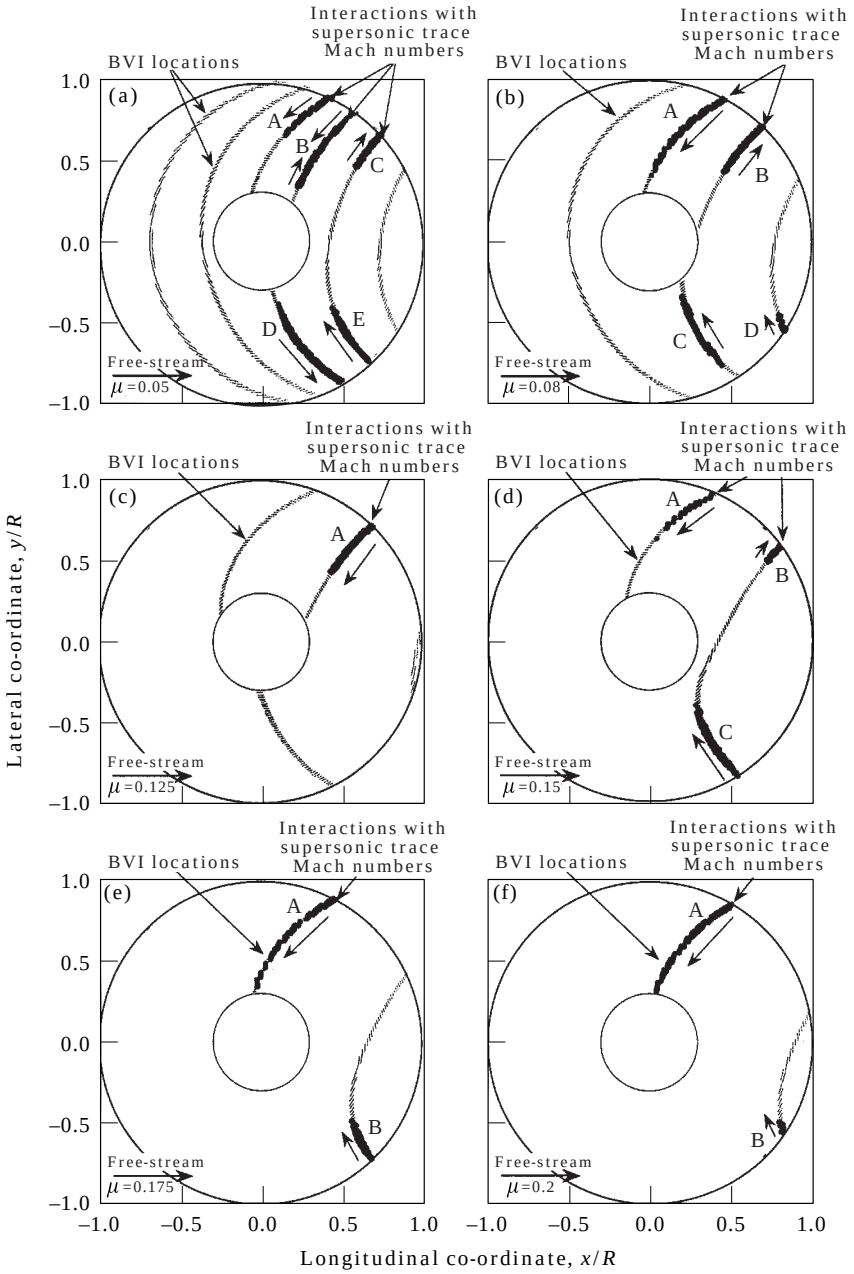

Figure 11. Locus of BVI locations and regions on the disk with supersonic trace Mach numbers for a one-bladed rotor operating at: (a) $\mu = 0{\cdot}05$, (b) $\mu = 0{\cdot}08$, (c) $\mu = 0{\cdot}125$, (d) $\mu = 0{\cdot}15$, (e) $\mu = 0{\cdot}175$ and (f) $\mu = 0{\cdot}2$.

corresponding acoustic lines and wave fronts. Note from Figure 12 the sensitivity of the sound directivity to relatively small changes in advance ratio. At the lower advance ratios, the blade tip vortices are not convected as quickly downstream away from the rotor so there are more potential BVIs that may occur over the rotor disk. At $\mu = 0{\cdot}05$—see Figure 11(a)—there are five BVI source clusters,

denoted by A through E. In this case the orientation of the tip vortices relative to the blade axis means that cluster B has both inward moving supersonic sources (parallel interactions with almost infinite trace Mach number) but also some outward moving sources (with somewhat lower trace Mach number).

Figure 12(a) shows that source clusters A and B are responsible for most of the focused sound waves, which emanate radially from the second and fourth quadrants of the rotor. The outward moving sources of cluster B also lead to some mild sound radiation from the third quadrant. On the retreating side, clusters D

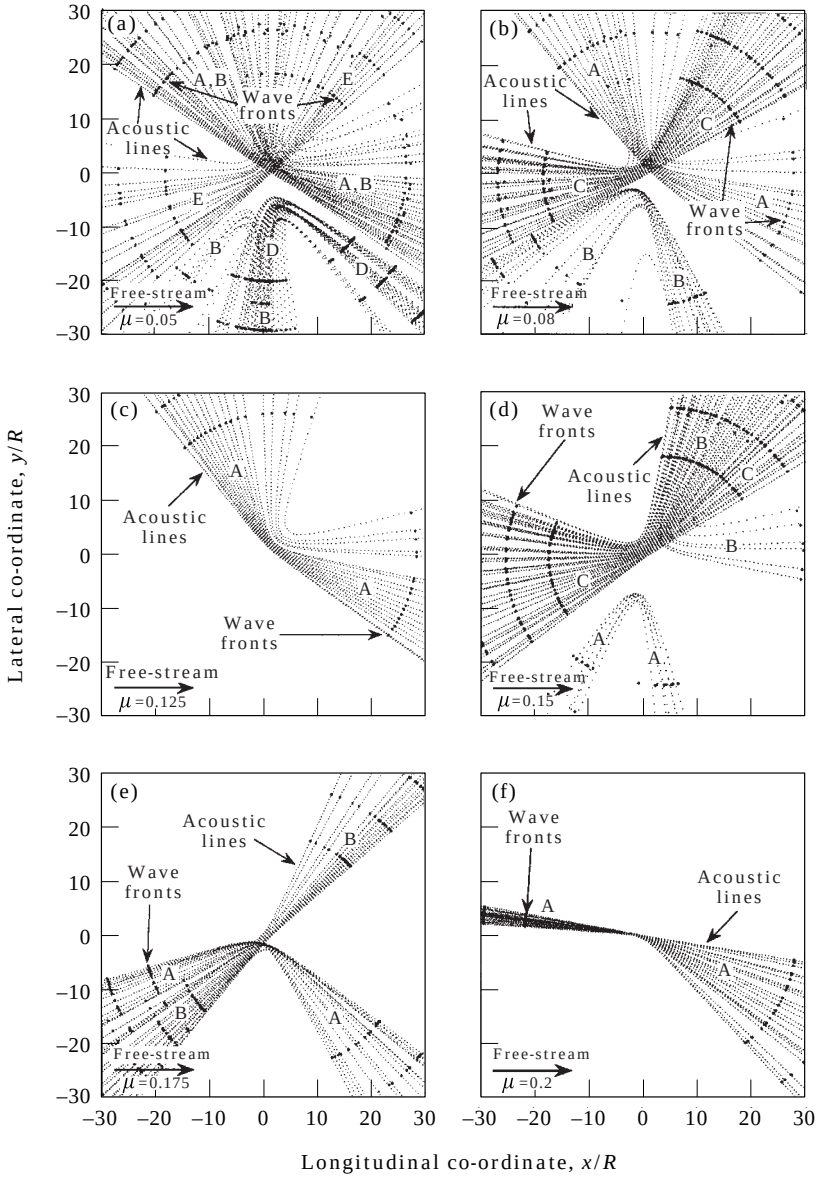

Figure 12. Acoustic lines and critical wave fronts for a one-bladed rotor operating at: (a) $\mu = 0{\cdot}05$, (b) $\mu = 0{\cdot}08$, (c) $\mu = 0{\cdot}125$, (d) $\mu = 0{\cdot}15$, (e) $\mu = 0{\cdot}175$ and (f) $\mu = 0{\cdot}2$. Observer plane located $3R$ below rotor.

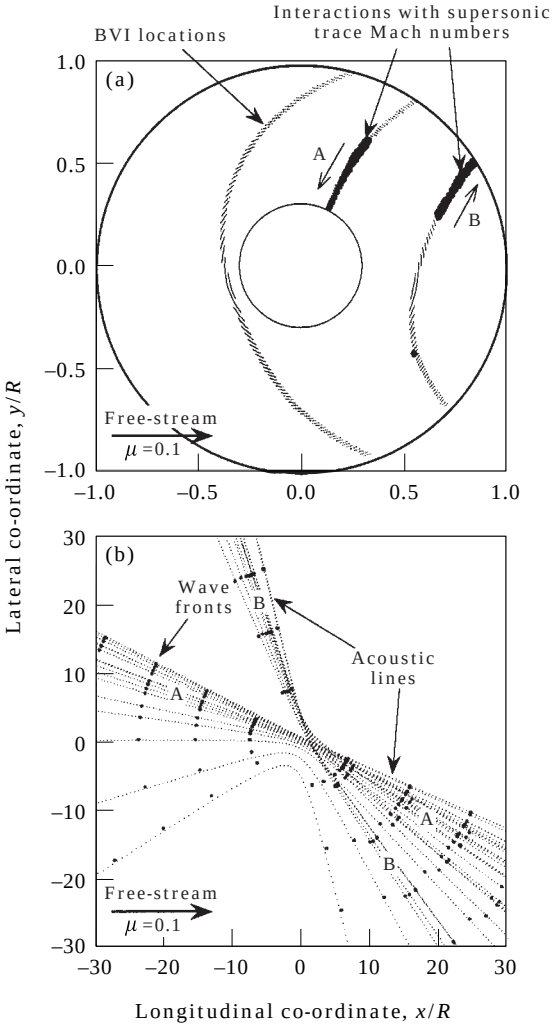

Figure 13. (a) BVI locations for a one-bladed rotor with a 30-degree swept back tip operating at an advance ratio of 0·1. (b) Corresponding acoustic lines and principal sound wave fronts. Observer plane located 3R below rotor.

and E represent outward and inward moving supersonic source clusters, respectively. Cluster D produces focused sound radiation from the third quadrant, while cluster E with the higher trace Mach number radiates sound from the first and third quadrant.

Increasing the advance ratio by only 0·03 to $\mu = 0{\cdot}08$ reduces significantly the number of potential BVI locations, and Figure 11(b) shows that there are now four main BVI clusters with supersonic trace Mach numbers. For this advance ratio the BVIs on the advancing side of the disk become less parallel to the tip vortices, so the trace Mach numbers are lower. Therefore, Figure 12(b) shows that the sound radiation from cluster A is well scattered into the advancing side of the rotor, with the sound from cluster B radiating from the retreating side. The most

parallel BVIs now occur from cluster C on the retreating side of the rotor disk, which results in sound radiation from the first and second quadrants.

Increasing the advance ratio to 0·125 produces only one BVI cluster with supersonic trace Mach numbers, as shown in Figure 11(c). Here the phase velocity is radially outward along the blade, and Figure 12(c) shows that the focused sound is radiated from the second and fourth quadrants of the rotor. Increasing the advance ratio to 0·15 continues to decrease the number of potential BVIs. However, it can be seen now from Figure 11(d) that three supersonic BVI clusters reappear. Clusters A and B are fairly oblique BVIs, and little focused sound occurs. However, cluster C on the retreating side shows a much more parallel interaction. Figure 12(d) shows that, like the previous cases, this interaction radiates sound from the first and third quadrants of the rotor.

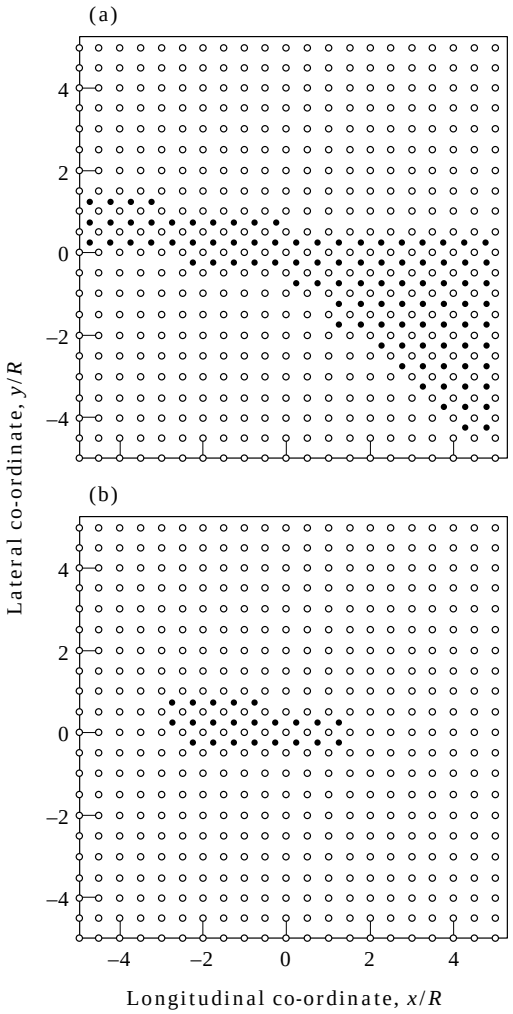

Figure 14. Example of a Cartesian acoustic field grid adapted on the basis acoustic line density. (a) Method M1—pure acoustic line density weighting. (b) Method M2—acoustic line density, inverse square, and Doppler weighting. ○, Basic grid; ●, adapted grid.

Further increases in advance ratio to 0·175 and 0·2—see Figures 11(e) and (f) and Figures 12(e) and (f), respectively—produces a more parallel BVI cluster on the advancing blade. Increasing the advance ratio by only 0·025 to $\mu = 0{\cdot}2$ produces a significant change in the directivity. Figure 11(f) shows that the curvature of the tip vortex is such that several BVI events are now essentially parallel to the blade as it sweeps over the vortex. The resulting trace Mach numbers are high, and Figure 12(f) shows that the sound is well focused forward of the rotor. This latter case is a situation where the retarded time values for source points on BVI cluster A are almost equal. That is the sound waves that arise at the point of intersection as the vortex sweeps along the blade all arrive on the acoustic lines A at the same instant in time. This can also be shown from an examination of the acoustic planform for the rotor.

3.3. PASSIVE SOUND DEFOCUSING STRATEGIES

The preceding results suggest some interesting possibilities for BVI sound reduction. One is simply to alter the operational advance ratio when noise becomes an issue. The sensitivity of the directivity to advance ratio, as shown above, suggests that an optimum flight condition when sound sources dephase in an acceptable way may indeed be possible. Such issues have been explored by Lowson [13] and Schmitz [19], although a proper optimal condition can only be found if the proximity of the wake to the rotor is properly modelled, i.e., by means of a free vortex wake [11, 12]. Also, because the unsteady airloads during the BVIs are required, it seems likely that a rigorous rotor model including blade flexibilities and structural dynamic modelling would be necessary prerequisites to any realistic assessment of such conditions. Currently, this is beyond the state-of-the-art.

It can be shown that the interesting curved nature of the rotor acoustic planform suggests that sweeping the blade planform either forward or backward, especially in the tip region, may help dephase the BVI sound signals at a given observer location. Alternatively, this can be viewed as simply changing the BVI trace Mach number; this will alter the radiation cone angles and may well defocus the sound and/or spread the acoustic energy in other principal directions. However, the main problem is to decrease the intensity or defocus the sound in one direction but without refocusing the sound elsewhere. The latter may result on the swept blades from new BVI locations with supersonic trace Mach numbers that may occur at other blade azimuth angles and/or other operational conditions, i.e., at a different advance ratio. Baeder [18] has approached the problem of using blade sweep to reduce BVI noise using CFD calculations of the blade airloads coupled with a FWH solution for the acoustics. Although noise reductions seem possible, the approach has not been applied to the epicycloidal tip vortex trajectories found with rotors. Therefore, the results still remain inconclusive.

The essential acoustics and directivity associated with blade sweep are readily examined using wave tracing. For simplicity, results for a constant 30-degree aft swept tip with the sweepback starting at 70% rotor radius are shown. The results in Figure 13 are for a rotor advance ratio of 0·1, and can be compared with the results for the unswept rotor blade shown in Figure 10. Note that at BVI cluster A, the blade tip sweep effectively eliminates the supersonic phase Mach numbers

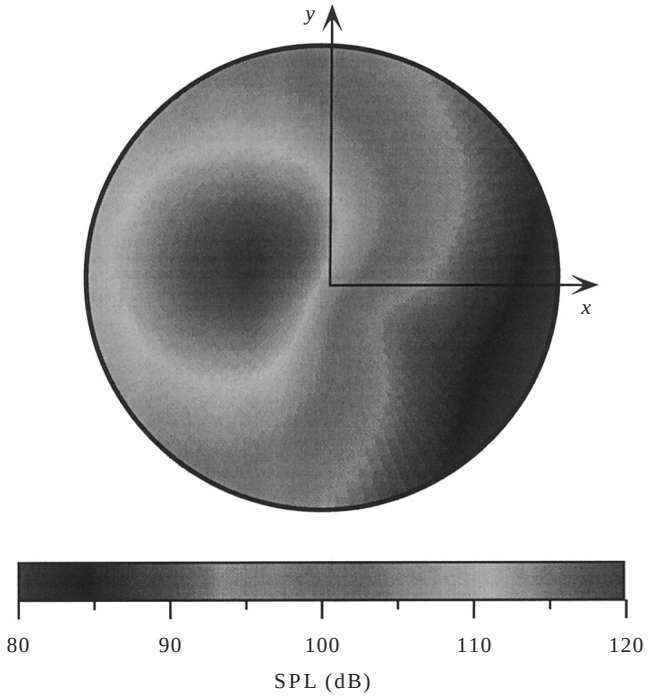

Figure 15. SPL levels resulting from loading noise as predicted by a FW-H model for the self-induced vortex wake of a one-bladed rotor operating at $\mu = 0{\cdot}2$. Observer plane at $z/R = -3R$. Field extends to $5R$.

near the tip. Also, BVI cluster C is all but eliminated. However, the sweepback increases the extent and magnitude of the trace Mach numbers found at cluster C. This is because here the tip vortices are more parallel to the leading-edge of the swept tip. These effects are manifest in the wave traces shown in Figure 13, where it will be apparent that, compared to the baseline (unswept blade) in Figure 10, the swept blade tip decreases the intensity of the wave fronts that are propagated along the acoustic lines A. However, the increase in the size of BVI cluster B also results in the formation of a new and well focused set of acoustic lines. This is the potential pitfall of such passive devices such as blade sweep; an optimal advance ratio may be too specific to be useful specifically for BVI noise reduction.

The preceding results confirm the complexity of the rotor acoustic problem and the need to carefully examine passive design concepts such as blade sweep from an overall design perspective. However, the computational efficiency of wave tracing analyses suggests coupling with an optimization routine may be a viable approach. It may be that an optimum distribution of sweep and flight condition can be found for minimum noise, or at least one where the noise is refocused in a more desirable way. The complete analysis, however, is a rather formidable undertaking because the proximity of the wake to the rotor would need to be included, i.e., a free vortex wake and structural dynamic model would need to be included in the optimization process. Nevertheless, even without structural dynamic modelling, it is a problem where further research will be fruitful.

3.4. REDISTRIBUTIVE OBSERVER GRID GENERATION

One advantage of wave tracing is that the main directivity of a subset of the acoustic field that result from BVIs can be quickly established. While the sound field is omnidirectional, the trace Mach number technique allows the focusing and primary propagation paths of the acoustic rays to be determined. This suggests that the method can be used as a pre-processor to help establish critical locations in the acoustic field that experience strong directivity and focusing effects. For example, observer points on a normally regular Cartesian or polar grid, as might be used with a FWH or Kirchhoff method, can be redistributed or adapted to more adequately capture the critical sound pressure regions. Also, because wave tracing will help define observer points with relatively low noise or weak directivity, computational wavings can be gained by using fewer observer points in these regions.

A simple example of the redistributed or adaptive grid procedure is shown in Figure 14(a) for a Cartesian observer field. The normally regular grid has been adapted on the basis of wave tracing for an advance ratio of 0·2, as shown previously in Figure 12(f). This is done by giving a high weighting to regions in the field with high acoustic line density and strong directivity originating with supersonic BVI trace Mach numbers. Only sound waves that actually reach the trajectories defined by the acoustic lines need be considered. The resulting grid points, therefore, become clustered in regions of more highly focused acoustic energy.

The second example shown in Figure 14(b) is another form of weighted grid. Here, redistributed observer points defined on the basis of the acoustic lines are further weighted by an inverse square law and a Doppler factor. It will be seen that this second procedure weights the observer points more heavily into the region of highest acoustic energy (cf. Figure 12(f)) and will be the preferred method.

The results of this wave tracing exercise are confirmed by the corresponding FWH analysis for the same operating conditions, as shown by the SPLs in Figure 15. Only the contributions from dipole "loading" noise are shown; the monopole noise associated with blade thickness has been removed from the calculation. It will be seen that the peak sound pressure lobe is very closely correlated with the directions obtained through wave tracing.

These simple wave tracing strategies ensure that there is a sufficiently high density of observer points to avoid missing the peak sound levels. Alternatively, the density of observer points with relatively low noise and/or completely free of focusing effects can be reduced, thereby saving computational cost in a directivity calculation. In the examples shown here, it is possible to reduce the number of observer points from 41 by 41 ($=1681$) to $(21 * 21) + 96 = 537$ points (using method A) or $(21 * 21) + 21 = 462$ points (method B) for essentially the same predictive resolution if wave tracing is first used to map the primary directivity. This represents a significant overall saving in computational cost when mapping out the acoustic field using FWH or Kirchhoff based acoustic methods.

4. CONCLUSIONS

This article has presented some results from a study of parallel and oblique blade vortex interactions (BVI). Examples of the idealized problem with an isolated line vortex as well as self-generated epicycloidal vortices have been considered. The results emphasize the complexity of the sound generation from helicopter rotors and the need to fully understand the nature of the BVI problem before embarking on paths that may lead to effective strategies for sound reduction.

As shown by Lowson and others, the trace Mach number model wave is an efficient way of mapping the main directivities (principal directions) of the acoustic field generated by BVI noise sources produced by a helicopter rotor. By determining blade/vortex intersection points over the rotor disk that have supersonic trace Mach numbers, the directivity of principal sound waves from these BVIs can be found with relatively low computational cost. The further application of wave tracing can help identify regions of focused sound, that is sound from multiple BVI source points that may have the same arrival time at an observer. The results are compared and contrasted with a solution obtained from the FWH equation, which has confirmed the nature of the wave front coalescence and how the BVI events can produce strongly directed noise in the far field. However, it is also noted that BVI source points with subsonic trace Mach numbers and the effects of "thickness" noise produce significant sound directivities that cannot be overlooked.

As a means of defocusing rotor noise, it has been shown that blade tip sweep may be a viable passive means of BVI sound reduction. However, the complex nature of the rotor tip vortex trajectories means that such a concept may only be a point design and further studies must be pursued. Finally, it has been shown how the trace Mach number approach combined with wave tracing can help design the acoustic grid so that it can be redistributed or adapted to more densely cover observer points associated with strong directivity. This can help avoid missing key regions with focused sound waves, or can help reduce the total number of observer points required with a FWH or Kirchhoff method to adequately resolve the sound directivity of helicopter rotors.

ACKNOWLEDGMENTS

Part of this work was supported by the US Army Research Office (ARO) under the 1996 MURI on Advanced Active Control of Rotorcraft Vibration and Acoustics.

REFERENCES

1. M. V. Lowson 1992 *Aeronautical Journal* **96**, 209–223. Progress towards quieter civil helicopters.
2. F. H. Schmitz 1991 *NASA Reference Publication* 1258. *Aeroacoustics of Flight Vehicles*: *Theory and Practice*. Chapter 2. Rotor noise.
3. A. R. George 1978 *Journal of Aircraft* **15**, 707–715. Helicopter noise: state-of-the-art.
4. F. W. Schmitz and Y. H. Yu 1986 *Journal of Sound and Vibration* **109**, 361–422. Helicopter impulsive noise: theoretical and experimental status.

5. B. W.-C. Sim, J. G. Leishman, R. C. Strawn and A. R. George 1997. *AIAA Paper* 97-1706. Analytical and computational investigations of oblique blade–vortex interaction generated noise.
6. F. Caradonna, C. Kitaplioglu, M. McCluer, J. Baeder, J. G. Leishman, C. Berezin, C. J. Bridgeman, C. Burley, R. Eipstein, A. Lyrintzis, E. Koutsavdis, G. Rahier, J. Jobard and J. Rule 1997 *American Helicopter Society Technical Specialist's Meeting in Rotorcraft Acoustics and Aerodynamics*, *Williamsburg*, *VA*. A review of methods for the prediction of BVI noise.
7. Y. H. Yu, Y. B. Gmelin, B. H. Heller, J. J. Philippe, E. Mercker and J. S. Preisser 1994 *Paper* 115, 20*th European Rotorcraft Forum*, *Amsterdam*, *The Netherlands*. Higher harmonic control aeroacoustics test—the joint German/French/US HART project.
8. D. Nance and L. N. Sankar 1997 *AIAA Journal* **35**, 255–262. Low dispersion finite volume scheme for aeroacoustic applications.
9. A. S. Lyrintzis 1994 *Journal of Fluids Engineering* **116**, 665–675. The use of Kirchhoff's method in computational acoustics.
10. R. C. Strawn 1997 *Journal of Aircraft* **34**, 665–672. New computational methods for the prediction and analysis of helicopter noise.
11. A. Bagai and J. G. Leishman 1995 *Journal of the American Helicopter Society* **40**, 29–41. Rotor free-wake modelling using a pseudo-implicit technique—including comparisons with experiment.
12. A. Bagai and J. G. Leishman 1995 *Journal of Aircraft* **32**, 1276–1285. Rotor free-wake modelling using a pseudo-implicit relaxation algorithm.
13. M. V. Lowson 1996 *Journal of Sound and Vibration* **190**, 477–484. Focusing of helicopter BVI noise.
14. B. W.-C. Sim, A. R. George and S. J. Yen 1995 *American Helicopter Society Aeromechanics Specialist Conference*, *Fairfield County*, *CT*. Blade–vortex interaction noise studies using the trace Mach number.
15. T. F. Brooks, E. R. Booth, D. D. Boyd, W. R. Splettstoesser, K. J. Schultz, N. Roland, H. Georg and O. Stregy 1991 *International Technical Specialists Meeting on Rotor Acoustics and Rotor Fluid Dynamics*, *AHS/RAeS*, *Philadelphia*, *PA*. HHC study in the DNW to reduce BVI noise—an analysis.
16. A. A. Hassan, L. N. Sankar and H. Tadghighi 1994 *Journal of the American Helicopter Society* **39**, 35–46. Effects of leading and trailing-edge flaps on the aerodynamics of airfoil/vortex interaction.
17. S. Dawson 1995 *American Helicopter Society*, 51*st Annual Forum*, *Fort Worth*, *TX*. Wind tunnel test of an active flap rotor: BVI noise and vibration reduction.
18. J. D. Baeder 1997 *American Helicopter Society* 53*rd Annual Forum*, *Virginia Beach*, *VA*. Passive design for isolated blade–vortex interaction noise.
19. F. H. Schmitz 1998 *Journal of the American Helicopter Society* **43**, 14–24. Reduction of blade vortex interaction (BVI) noise through X-force control.
20. M. V. Lowson and J. B. Ollerhead 1968 *USAAVLABS Technical Report*, 68–60. Studies of helicopter rotor noise.
21. T. D. Ringler, A. R. George and J. B. Steele 1991 *American Helicopter Society's International Technical Specialist Meeting*, *Valley Forge*, *PA*. The study of blade–vortex interaction sound generation and directivity.
22. B. W.-C. Sim and A. R. George 1996 2*nd AIAA/CEAS Aeroacoustics Meeting*, *State College*, *PA*. The propagation of caustics in rotorcraft blade–vortex interaction noise.
23. S. Widnall 1971 *Journal for the Acoustical Society of America* **50**. Pt. 2. Helicopter noise due to blade–vortex interaction.
24. R. O. Onyenonwu 1975 *Journal of Sound and Vibration* **42**, 85–102. Sonic boom signatures and ray focusing in general manoeuvres: 1. Analytical foundations and computer formulation.

25. R. O. Onyenonwu 1975 *Journal of Sound and Vibration* **42**, 103–114. Sonic boom signatures and ray focusing in general manoeuvres: 2. Numerical study.
26. M. Surendraiah 1970 *NASA CR*-1573. An experimental study of rotor blade–vortex interaction.
27. F. X. Caradonna, G. H. Laub and C. Tung 1984 *Workshop on Blade Vortex Interaction*, *NASA Ames Research Center*. An experimental investigation of the parallel blade–vortex interaction.
28. T. Kokkalis and R. A. McD. Galbraith 1986 *Paper* 80, 12*th European Rotorcraft Forum*, *Garmish*, *Germany*. Description of and preliminary results from a new blade–vortex interaction test facility.
29. D. D. Seath, J. M. Kim and D. R. Wilson 1987 *AIAA Paper* 87-1344, 19*th Fluid Dynamics*, *Plasma Dynamics and Lasers Conference*, *Honolulu*. An investigation of the parallel blade–vortex interaction in a low speed wind-tunnel.
30. C. Kitaplioglu and F. X. Caradonna 1994 *American Helicopter Society Aeromechanics Specialists Conference*, *San Francisco*, *CA*. F.X. Aerodynamics and acoustics of blade vortex interaction using an independently generated vortex.
31. C. Kitaplioglu, F. X. Caradonna and C. L. Burley 1997 *Journal of the American Helicopter Society* **42**, 272–281. Parallel blade–vortex interactions: an experimental study and comparison with computation.
32. J. E. Ffowcs-Williams and D. L. Hawkins 1969 *Philosophical Transactions of the Royal Society of London* **A264**, 321–342. Sound generation by turbulence and surfaces in arbitrary motion.
33. J. G. Leishman 1996 52*nd Annual Forum of the American Helicopter Society*, *Washington*, *DC*. Aeroacoustics of 2-D and 3-D blade vortex interaction using the indicial method.
34. J. G. Leishman 1996 22*nd European Rotorcraft Forum*, *Brighton*, *England*. Aeroacoustics of blade vortex interaction using the indicial method and the acoustic analogy.
35. F. Farassat 1981 *AIAA Journal* **19**, 1122–1130. Linear acoustic formulas for calculation of rotating blade noise.
36. J. M. Gallman 1990 *NASA TM*-101793. The validation and application of a rotor acoustic prediction computer program.
37. J. G. Leishman 1997 *Journal of Aircraft* **34**, 719–729. Unsteady aerodynamics of airfoils encountering traveling gusts and vortices.